



Article

A 40 Mb/s VLC System Reusing an Existing Large LED Panel in an Indoor Office Environment

Xicong Li ¹ , Zabih Ghassemlooy ¹ , Stanislav Zvanovec ²  and Paul Anthony Haigh ³ 

¹ Optical Communications Research Group, Faculty of Engineering and Environment, Northumbria University, Newcastle upon Tyne, NE1 8ST, UK; [xicong.li; z.ghassemlooy]@northumbria.ac.uk

² Department of Electromagnetic Field, Faculty of Electrical Engineering, Czech Technical University in Prague, Prague, Czech Republic, 16627; xzvanove@fel.cvut.cz

³ Intelligent Sensing and Communications Group, School of Engineering, Newcastle University, Newcastle upon Tyne, NE1 7RU, UK; paul.haigh@newcastle.ac.uk

* Correspondence: xicong.li@northumbria.ac.uk;

† This paper is an extended version of our paper published in the 12th International Symposium on Communication Systems, Networks and Digital Signal Processing (CSNDSP), Porto, Portugal, 20-22 July, 2020.

Abstract: With advances in solid-state lighting, visible light communication (VLC) has emerged as a promising technology to enhance existing light-emitting diode (LED)-based lighting infrastructure by adding data communication capabilities to the illumination functionality. The last decade has witnessed the evolution of the VLC concept through global standardisation and product launches. Typically deploying VLC systems requires replacing existing light sources with new luminaires equipped with data communication functionality. To save the investment, it is clearly desirable to make the most of the existing illumination systems. This paper investigates the feasibility of adding data communication functionality to the existing lighting infrastructure. We do this by designing an experimental system in an indoor environment based on an off-the-shelf LED panel typically used in office environments, with dimensions of 60×60 cm². With minor modifications, the VLC function is implemented, and all the modules of the LED panel are fully reused. A data rate of 40 Mb/s is supported at a distance of up to 2 metres using the multi-band carrierless amplitude and phase (CAP) modulation. Two main limiting factors for achieving higher data rates are observed. The first factor is the limited bandwidth of the LED string inside the panel. The second is the flicker due to the residual ripple of the bias current generated by the panel's driver. Flicker is introduced by the low-cost driver, which provides bias currents that fluctuate in the low frequency range (less than several kilohertz). This significantly reduces the transmitter's modulation depth. Concurrently, the driver can also introduce an effect similar to baseline wander at the receiver if the flicker is not completely filtered out. We also proposed a solution based on digital signal processing (DSP) to mitigate the flicker issue at the receiver side and its effectiveness has been confirmed.

Keywords: visible light communication; LED; carrierless amplitude and phase modulation (CAP); LED driver; bias-tee; lighting infrastructure

Citation: Li X.; Ghassemlooy, Z.; Zvanovec, S.; Haigh, P. A 40 Mb/s VLC System Reusing an Existing Large LED Panel in an Indoor Office Environment. *Sensors* **2021**, *1*, 0. <https://doi.org/>

Received:

Accepted:

Published:

Publisher's Note: MDPI stays neutral with regard to jurisdictional claims in published maps and institutional affiliations.

Copyright: © 2021 by the authors. Submitted to *Sensors* for possible open access publication under the terms and conditions of the Creative Commons Attribution (CC BY) license (<https://creativecommons.org/licenses/by/4.0/>).

1. Introduction

Visible light communication (VLC) has attracted continued research interest [1–3] while solid-state lighting has dominated the mass market over the last two decades [4]. The use of solid-state semiconductor devices such as light-emitting diodes (LEDs), organic light-emitting diodes (OLEDs) [5–7] and laser diodes (LDs) [8,9] in the visible range enables intensity modulation of the optical power for communication simultaneously with illumination. Therefore, the VLC technology has the potential to reuse the existing lighting infrastructure to deliver add-on functionality in a cost-effective manner that can be adopted in future smart indoor and outdoor environments. The outdoor

lighting infrastructure covers a variety of LED-based luminaries ranging from street lights, traffic lights to car lights, which have inspired the use of VLC in infrastructure-to-vehicular (I2V) and vehicular-to-vehicular (V2V) communications [10,11]. Experiments using existing traffic lights and car lights as transmitters have been reported to demonstrate the feasibility of VLC in the outdoor I2V/V2V communications [12,13]. Compared with the outdoor environment, the indoor scenarios often find large LED luminaries installed in the ceiling or relatively small LED desk lamps placed directly above the table to provide a guaranteed light level for illuminance. This benefits the indoor VLC applications greatly since those LED luminaries' high output optical power can ensure a decent signal-to-noise (SNR) profile within rooms/offices if their intensity is efficiently modulated. In this work, we hereafter limit the scope to VLC deployment in the indoor environment because of its advantages and popularity.

Motivated by the potential of VLC, standardisation has been carried out by several organisations [14–16]. Recent standardisation activities are mainly conducted within the Institute of Electrical and Electronics Engineers (IEEE) and the International Telecommunication Union Telecommunication Standardisation Sector (ITU-T) [16]. In March 2017, the IEEE 802.15.13 task group was established with the goal to define an optical wireless communication (OWC) standard that supports data rates of up to 10 Gb/s using wavelength ranging from 190 to 10000 nm. The first draft was finished in 2019 with a letter ballot held in 2020. The standard is expected to be completed in 2021. In parallel with 802.15.13, the IEEE 802.11bb task group was formed in May 2017 to develop a global OWC standard targeted at the mass market within the well-known IEEE 802.11 wireless local area networks (WLAN, which is often linked and used interchangeably with WiFi, i.e. wireless fidelity) standard family. Since latest standards typically define communications operating in the band beyond the visible light spectrum, the concept of light fidelity (LiFi), which covers both visible and infrared bands, has been introduced [17]. The ambition of 802.11bb is to operate as closely as possible to the base 802.11 standards to allow integration with WLAN chipset vendors. Consequently, the physical (PHY) layer of 802.11a with a bandwidth of 20 MHz has been adopted as the common PHY mode in 802.11bb. The draft is still under discussion and expected to be completed in 2021. As another influential standardisation body, ITU-T published a new VLC/LiFi standard G.9991 (also known as G.vlc) [18] in 2019, which is highly based on the ITU-T's high-speed power-line communication standard G.9960 (also known as G.hn) [19,20]. In the PHY layer, G.9991 defines two PHY modes which employ the orthogonal frequency division multiplex (OFDM) modulation with three band plans. The total bandwidth in the three band plans is 50, 100, and 200 MHz, respectively. A maximum data rate of 2 Gb/s is supported. Since the release of G.9991, several chipset implementations have been available from the G.hn semiconductor vendors, helping accelerate VLC/LiFi applications in the real world [16].

Nevertheless, not much attention has been paid to the viability and complexity of implementing VLC using the existing lighting infrastructure following the standardised specifications. Current commercial products normally require complete replacement of the existing illumination systems with new luminaires supporting VLC. It is therefore desirable to make the most of the existing illumination systems to save the investment and reduce the deployment cost. In this paper, we investigate the possibilities and challenges in upgrading the existing LED-based luminaries with VLC functionality by developing a demonstration system in a practical indoor environment. To the best of authors' knowledge, there exist limited reports on reusing the existing commercial LED luminaries for simultaneous VLC communication and illumination in the literature. In [21], a commercial LED table lamp was upgraded to a VLC system providing a 10Base-T Ethernet connection via an optical wireless transmission of 12.5 Mb/s Manchester coded on-off-keying (OOK) signals. Due to the transmission speed limitation of the Ethernet connection, the achievable system capacity is not fully exploited. Additionally, chal-

86 lenges and issues in implementing such a practical system based on existing luminaries
87 are not covered in [21].

88 Most of the indoor VLC systems reported in the literature are based on dedicated
89 designs using LEDs over a short distance in a controlled laboratory environment, fo-
90 cusing on achieving high data rates. Recent reported experimental systems have been
91 demonstrating transmission speed in the order of Gb/s with precisely aligned point-
92 to-point links based on single-colour LEDs (scLEDs) [22–24]. The use of the scLEDs
93 contributes significantly to the throughput in Gb/s since they offer higher modulation
94 bandwidth than the phosphor-converted white LEDs (pcwLEDs) with the absence of the
95 slow response phosphor. However, the existing illuminance products widely adopted
96 pcwLEDs due to their low cost, thus imposing hurdles to achieving comparable data
97 rates. As shown later, the LED panel adopted in our demonstration system consists of
98 240 pcwLEDs and has a 3-dB bandwidth of only 1.4 MHz. Although the bandwidth
99 of pcwLEDs can be increased to between 10 and 20 MHz by using blue filters at the
100 receiver side to mitigate the slow temporal response of the phosphor, this improvement
101 in bandwidth is paid for at the cost of power loss or signal-to-noise ratio (SNR) penalty
102 due to the phosphor-converted portion of the received light spectrum being filtered
103 out [25]. It is unnecessary to use blue filters if multi-carrier modulation schemes, espe-
104 cially with bit-loading, are applied because multi-carrier modulation can utilise all the
105 signal power in the full received light spectrum to achieve higher SNR and therefore
106 higher system capacity, or data rates [26]. Similarly, analogue pre-equalisers [27,28] are
107 designed to compensate for the frequency response of the LED to extend the normalised
108 3-dB bandwidth by sacrificing the modulation depth, which leads to the same issue as
109 using blue filters [29]. Hence, we adopted a multi-band carrierless amplitude and phase
110 modulation (CAP) [30–32] with bit-loading to combat the limited bandwidth problem
111 due to its simple implementation and low peak-to-average power ratio (PAPR) [33].

112 In addition, those high-speed experimental VLC systems often require bulky optics
113 to realise precise alignment between transmitters and optical receivers, which is unrea-
114 sonable for practical VLC applications in the real world. An optical receiver with a large
115 field of view (FoV) and sensitivity is a key enabling factor for the deployment of VLC
116 applications. We have designed and built a compact optical receiver with a half angle of
117 $\pm 35^\circ$, which highly relaxes the alignment requirement, to demonstrate the usability of
118 our system in real-world scenarios.

119 Another key challenge faced in our system is the flicker caused by the low-cost
120 LED driver. The residual current ripple from the LED driver introduces unwanted
121 low-frequency light intensity modulation and hence reduces the modulation depth
122 of VLC signals. To address the flicker issue, optimised LED driver circuits for VLC
123 have been proposed [34,35]. In this paper, we still use the existing LED driver with the
124 flicker problem in order to fully reuse the existing illumination system and keep the
125 modification within a minimum degree. The detrimental effect of flicker on a binary
126 phase modulation (BPM) VLC system is investigated in [36] under the condition that
127 the flicker is treated as random interference. In this paper, we treat the flicker as an
128 underlying stationary and predictable signal and therefore we can use a low-pass finite
129 impulse response (FIR) filter to filter out the low-frequency components as an estimate
130 of the flicker. After subtracting the estimated flicker from the received raw signal,
131 the adverse effects of flicker can be alleviated greatly, offering a different approach to
132 addressing the flicker at the receiver. Since the estimation of the flicker can be realised
133 by a programmable FIR filter in the digital domain, this digital signal processing (DSP)-
134 based solution can be applied universally to deal with a variety of flicker specifications.

135 Our demonstration system can support a data rate of 40 Mb/s at a distance of up
136 to 2 metres with a minimum illuminance level of 300 lux [37]. The VLC functionality is
137 added to the existing light infrastructure without any degradation in the lighting level,
138 presenting a usable VLC/LiFi system in an indoor office environment.

The remainder of this paper is organised as follows. In Section 2, the demonstration system is described in detail. Section 3 discusses the key challenges in the implementation of the proposed system and presents experimental results. Finally, conclusions are made in Section 4.

2. Experimental Setup

The proposed system block diagram and a photo of the experimental setup are shown in Figure 1. The lighting device used in our demonstration system is a 60×60 cm² commercial LED panel (DFx 563-004-01) which has been installed in our laboratory ceiling. We use a bias-tee circuit to modulate the LED panel's intensity with information-carrying signals generated by an arbitrary waveform generator (AWG) and place an optical receiver underneath connected to an oscilloscope (OSC) to capture the regenerated transmitted signals for offline MATLAB processing. To upgrade the LED panel with the data transmission function, full characterisation of the panel was performed, followed by modulation circuit design, modulation scheme design, and experimental test.

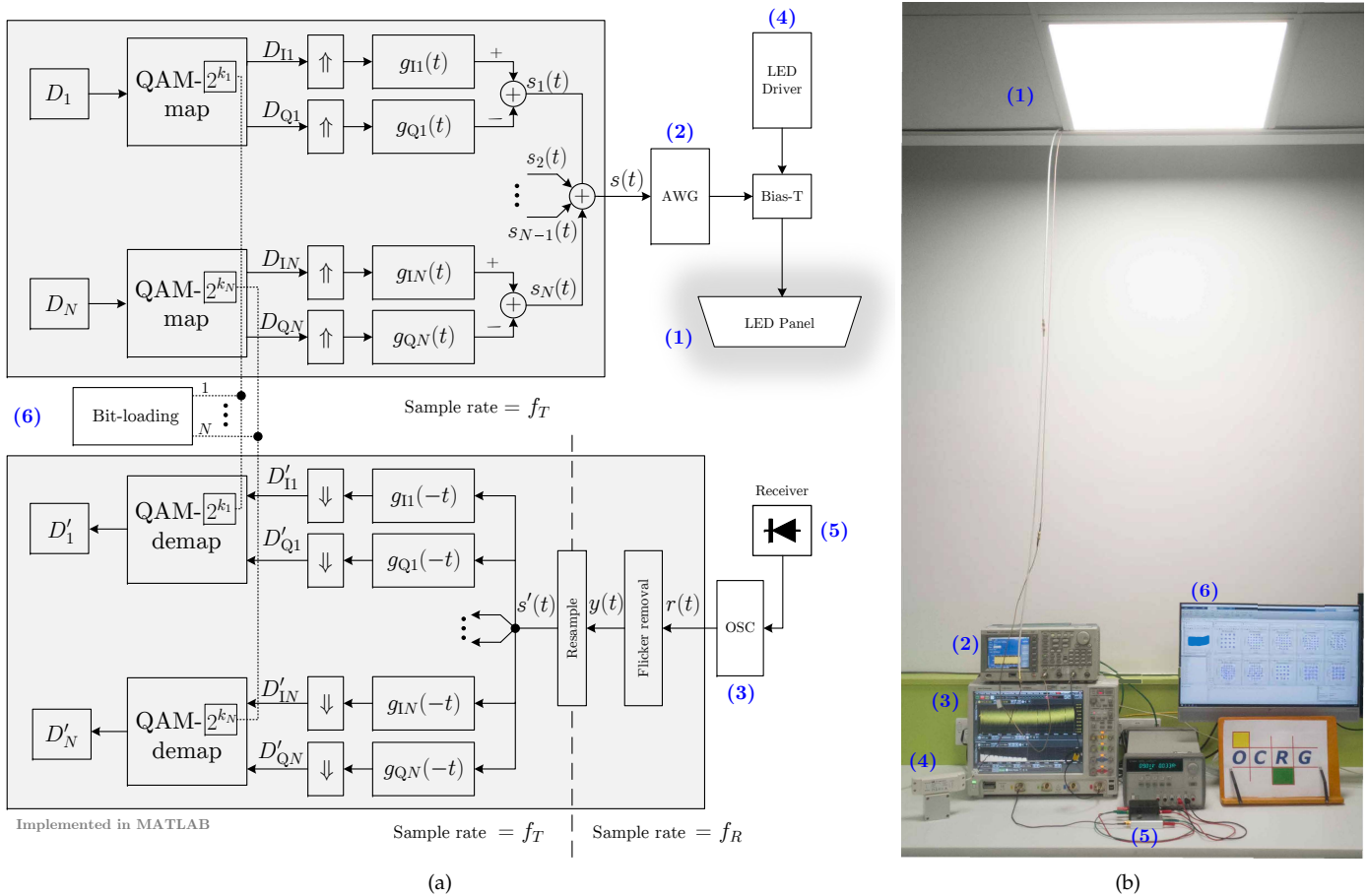


Figure 1. (a) System block diagram; (b) experimental setup.

2.1. The LED Panel

In Figure 2(a), the internal structure of the LED panel is depicted. Two LED strips are mounted on opposite sides of a square aluminium frame that hosts a transparent light guide plate to direct the light evenly within the panel area. On the backside of the light guide plate is a single layer of reflective paper used to redirect the optical power to the receiver plane. The other side of the light guide is attached to a diffuser plate

160 to produce evenly-distributed light for illumination. The two LED strips consist of 12
 161 serially connected blocks of 20 LEDs that are connected in parallel, see Figure 2(b).

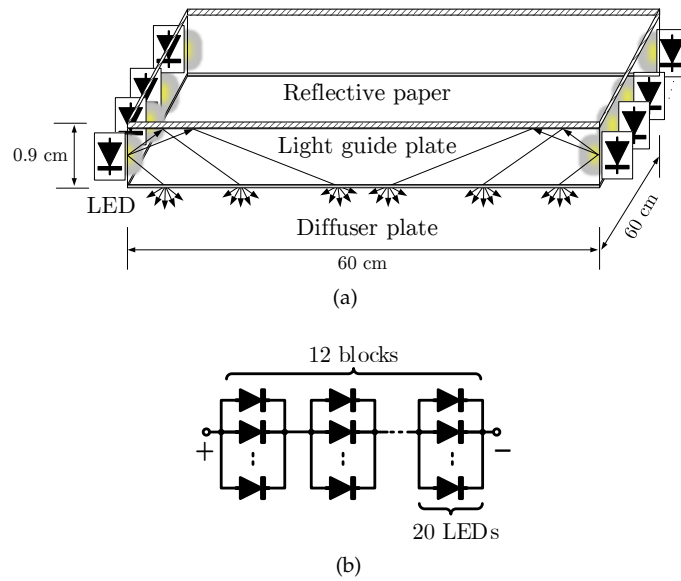


Figure 2. (a) Illustrative view, and (b) schematic of the LED panel in use.

162 2.2. LED Panel Driver and Characteristics

163 We utilised the existing LED panel driver and designed a bias-tee circuit as illus-
 164 trated in Figure 3, where the AC port of the bias-tee module is connected to an AWG for
 165 intensity modulation of the LED panel. Alternative LED drivers with low ripple/noise
 166 can be used depending on the system requirements, but with increased cost and com-
 167 plexity. To measure the V - I curve of the LED panel, two low-noise voltage sources were
 168 connected in series, as shown in Figure 4(a), to generate high enough voltages to turn on
 169 the LED strips. Since the turn-on voltage of each LED is around 2 V, the turn-on voltage
 170 for the entire LED string can be estimated to be ~ 24 V. Therefore, the first voltage source
 171 is set to a fixed voltage of 24 V, while the second is set to sweep voltage and monitor the
 172 corresponding current. The measured V - I curve of the LED panel as a lumped element
 173 is shown in Figure 4(b). From the datasheet, the LED panel is biased at 0.9 A with a
 174 corresponding voltage of around 34.5 V.

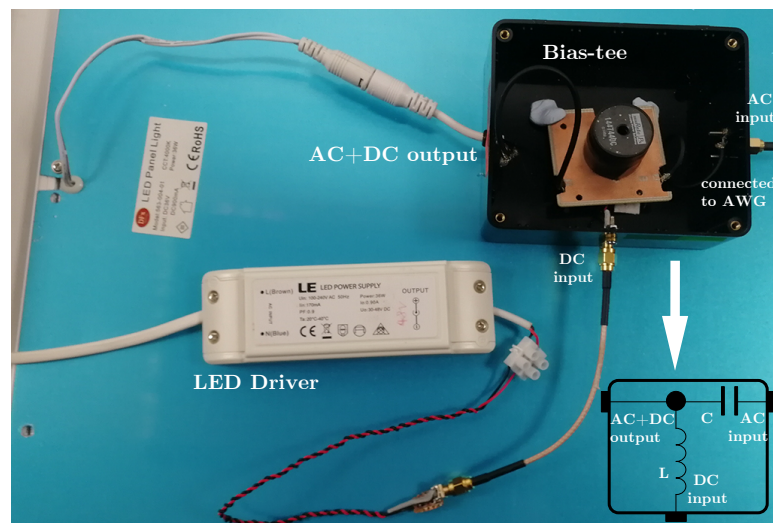


Figure 3. The bias-tee combining the LED driver and AWG to drive the LED panel.

Next, we measured the frequency response of the LED panel at the bias point of (34.5V, 0.9A) using the setup shown in Figure 5(a). Here, we used two low-noise voltage sources connected in series as in the V - I measurement to mitigate the light intensity flicker caused by the residual current ripple of the original LED panel driver. With an AWG and a spectrum analyser (SA), the frequency response is measured and plotted in Figure 5(b) with a 3-dB bandwidth of 1.4 MHz. The list of equipment for characterising the LED panel is given in Table 1.

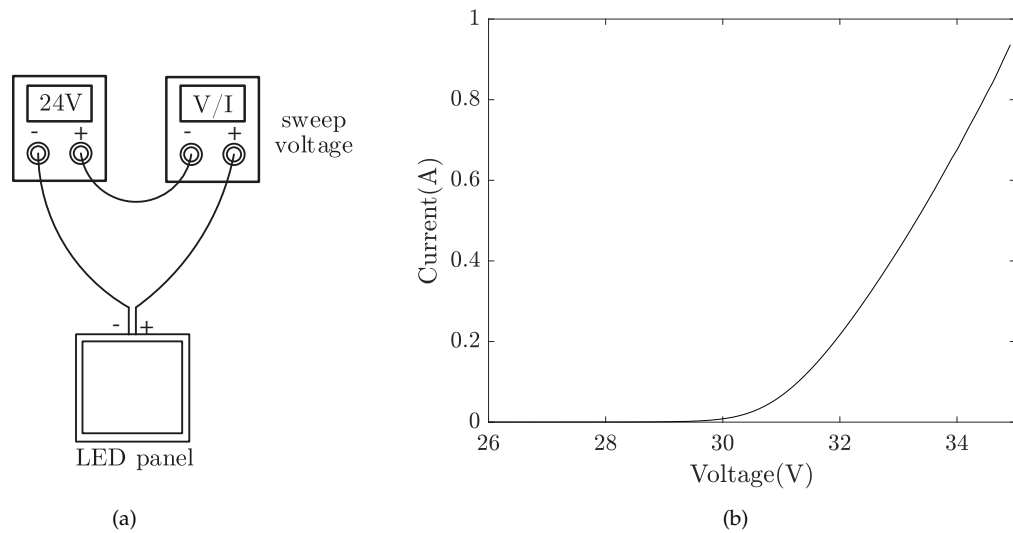


Figure 4. (a) Setup for V - I measurement; (b) measured V - I curve of the LED panel.

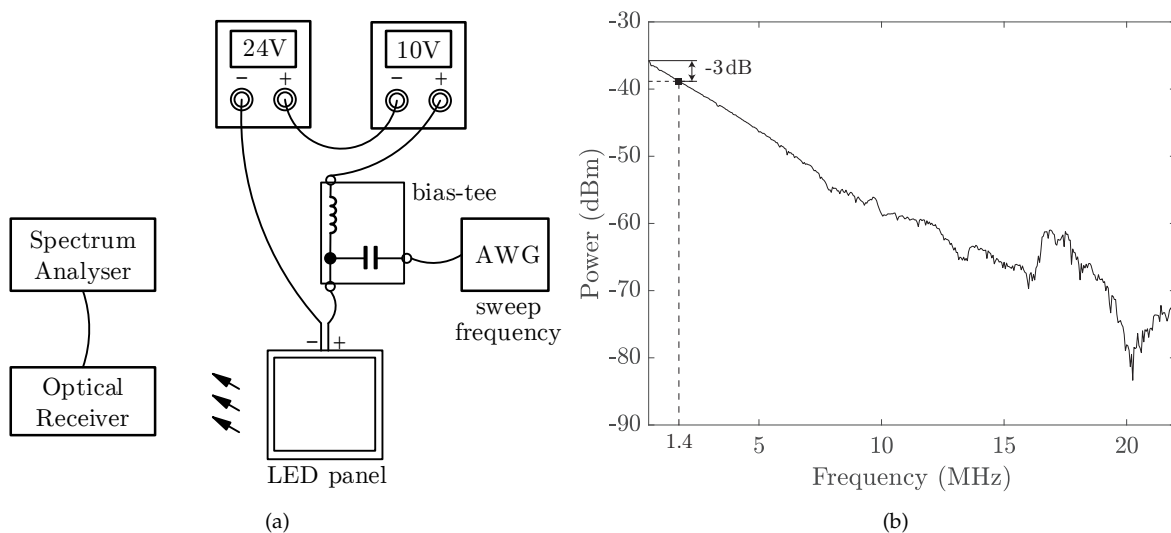


Figure 5. (a) Setup for frequency response measurement; (b) measured frequency response of the LED panel.

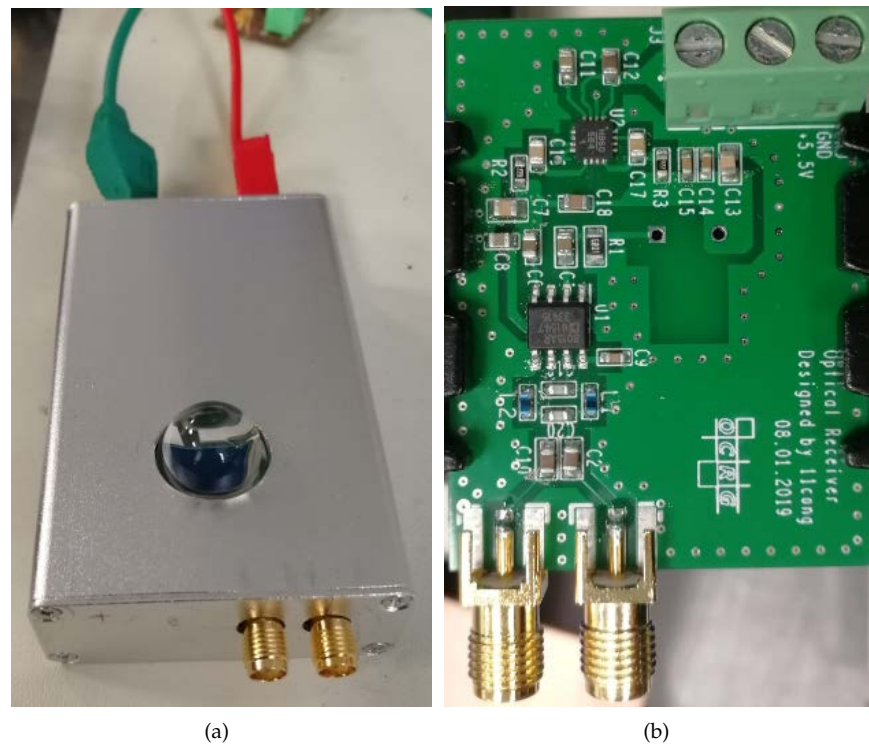
Table 1. The list of equipment.

Item	Value
LED panel model	DFx 563-004-01, 4000K, 36W
Lumens	2700 lm
Luminous Efficiency	75 lm/W
Voltage source	Keysight E3631A
AWG	Tektronix AFG3022
SA	Keysight N9020A

2.3. Optical Receiver

To relax the alignment requirement between the LED panel and the receiver, we adopted a silicon PIN photodiode (Hamamatsu S6968) with a large effective photosensitive area of 150 mm^2 and a built-in 14 mm (diameter) lens in the plastic package. A trans-impedance amplifier (TIA) circuit converts the detected current from the photodiode into a voltage signal with a gain of $10 \text{ k}\Omega$ for following data acquisition by the OSC. The optical receiver was implemented compactly using a printed circuit board (PCB) inside an aluminium enclosure. A photo of the optical receiver is given in Figure 6 with a closeup of the PCB inside.

Figure 7 depicts the receiver's relative signal strength at varying incident light angles, from which a half angle of $\pm 35^\circ$ can be observed. Here the half angle is defined as the incident angle at which the strength is reduced to half of that generated when the incident light is perpendicular to the photodiode. We also observed that the optical receiver works robustly as long as the LED panel shines it in our practical measurements. In addition, using a high-bandwidth laser diode (Osram, PL450B) as the light source, we measured the 3-dB bandwidth of our receiver is around 20 MHz, which satisfies our system specification.

**Figure 6.** (a) Optical receiver and (b) the PCB inside.

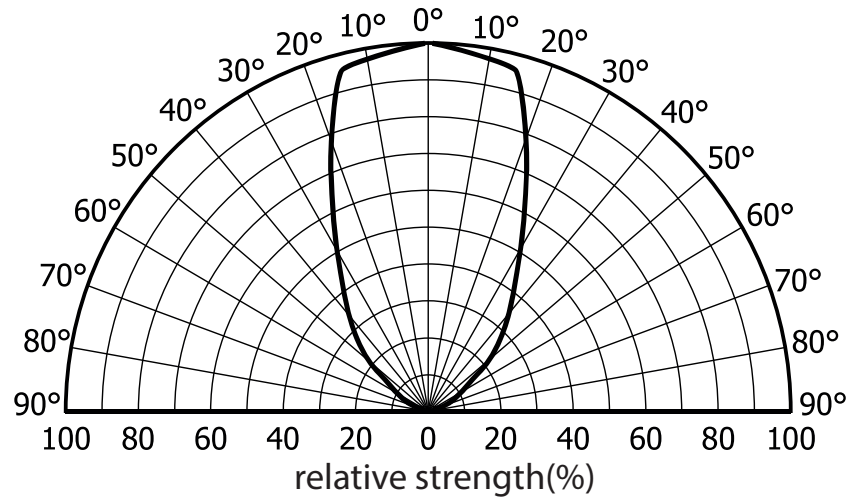


Figure 7. Measured directivity of the optical receiver.

2.4. MultiCAP for the Downlink VLC

It is well known that LEDs, especially those used for illumination, suffer from low 3-dB bandwidth (up to a few MHz) and decaying frequency responses [38], as shown in Figure 5(b). Unlike radio frequency (RF) wireless technologies where multi-path induced fading is highly critical, multi-path fading is not a major concern and poses limited impact on the overall system frequency response in indoor VLC systems. One main reason is that most practical indoor VLC systems are static line-of-sight (LOS) channels. The other reason is that the coherence bandwidth of a typical indoor non-LOS (NLOS) channel is much higher than the LED's 3-dB bandwidth, thus making the LED capable of approximately representing the frequency response of the entire VLC system. Recent experimental results have shown that a maximum root mean-square (RMS) delay spread of 14.2 ns was measured for a 3 m NLOS link in a worst practical indoor scenario [39,40]. The coherence bandwidth can be estimated to be in the order of several tens of MHz, which is still much higher than the LED panel's bandwidth of 1.4 MHz used in this work. To overcome the unideal channel response, a multi-carrier version of carrierless amplitude and phase (MultiCAP) modulation with bit-loading is adopted [41]. Compared with OFDM, MultiCAP has a lower peak-to-average power ratio (PAPR) because typical MultiCAP implementations tend to use a smaller number of carriers. In addition, modulation and demodulation of MultiCAP can be implemented with reduced complexity due to the absence of fast Fourier transform (FFT) and inverse FFT operations. The parameters and algorithms for the modulation and demodulation are described as follows.

Suppose a full band of B_{mod} is divided evenly into N sub-bands. Each sub-band is transmitting a band-pass CAP signal, which is similar to quadrature amplitude modulation (QAM). For example, the n^{th} sub-band is centred at the carrier frequency $f_n = \frac{2n-1}{2N}B_{\text{mod}}$, where $n = 1, \dots, N$. Since the band is divided evenly, the baseband symbol rate R_s in each sub-band is the same and is equal to $\frac{B_{\text{mod}}}{N(1+\beta)}$ when using the square-root raised cosine (SRRC) filter with a roll-off factor of β for pulse shaping. The MultiCAP filter bank consists of N pairs of pulse shaping filters as given by:

$$\begin{aligned} g_{In}(t) &= g(t) \cos 2\pi f_n t \\ g_{Qn}(t) &= g(t) \sin 2\pi f_n t \end{aligned} \quad (1)$$

where

$$g(t) = \frac{\sin[\pi(1-\beta)t/T_s] + 4\beta t/T_s \cos[\pi(1+\beta)t/T_s]}{\pi t/T_s [1 - (4\beta t/T_s)^2]}$$

is the SRRC pulse and $T_s = 1/R_s$ is the baseband symbol period. The synthesis of pulse shaping filters in (1) with built-in carriers is the major difference between CAP and QAM. Due to this feature, CAP does not require extra free-running oscillators and mixers to shift the spectrum to the target frequency range, which is beneficial when designing low-cost systems.

Block 6 of Figure 1(a) illustrates the schematic diagram for the implementation of modulation and demodulation in MultiCAP. At the transmitter, for the n^{th} sub-band, a random symbol sequence D_n is split into two branches, i.e., an in-phase (I) sequence D_{In} and a quadrature (Q) sequence D_{Qn} , after the QAM- 2^{k_n} constellation mapping. Here, k_n denotes the QAM constellation order (in bits) used in the n^{th} sub-band. Then the baseband symbol sequences D_{In} and D_{Qn} are up-sampled and filtered by the n^{th} in-phase and quadrature filters of $g_{In}(t)$ and $g_{Qn}(t)$, respectively. Finally, the n^{th} CAP signal is generated by subtracting the I path signal from the Q path signal, which is given by:

$$s_n(t) = D_{In} * g_{In}(t) - D_{Qn} * g_{Qn}(t) \quad (2)$$

where $*$ is the time-domain convolution. The MultiCAP signal is generated by summing up (2), which is expressed by:

$$s(t) = \sum_{n=1}^N s_n(t).$$

In our demonstration system, the MultiCAP signal is generated in MATLAB and up-loaded to the AWG, which produces a corresponding waveform at a sampling frequency of f_T to modulate the LED panel's intensity.

At the receiver, demodulation is carried out in the reverse order of the modulation. After the flicker removal and resampling operations, the signal $y(t)$, which is captured by the OSC at a sample frequency of f_R , turns to the signal $s'(t)$ which is ready for demodulation. The signal $s'(t)$ is first applied to N pairs of match filters with the pulse impulse response of $g_{In}(-t)$ and $g_{Qn}(-t)$, $n = 1, \dots, N$, and then down-sampled to recover the transmitted I/Q symbols. Following QAM constellation demapping, N streams of symbols $\{D'_n\}$ are obtained and compared with the transmitted data $\{D_n\}$ to calculate the symbol error rate (SER) or the bit error rate (BER). The selection of the QAM order k_n is realised using a simple bit-loading algorithm, which iteratively searches for the largest k_n capable of supporting a BER below the 7% forward error correction (FEC) limit of 3.8×10^{-3} . In our work, the determination of the bit-loading pattern was only carried out at the longest distance (2 metres), which has the worst SNR profile and can then support shorter distance with better BER performance.

Note that the flicker removal is to mitigate the baseline wander caused by the current ripple of the LED driver and will be detailed in the next section. Additionally, since the nominal frequency of f_R is not identical to f_T , a resampling process is applied to match the underlying sampling rate with that of the reference transmitted data. Using the demodulation algorithms described above, the recovered data stream is compared with the transmitted data to determine the BER. The key parameters adopted in this work are listed in Table 2.

Table 2. Key system parameters.

Item	Value
OSC	Keysight DSO9254A
AWG	Tektronix AFG3022
AWG output voltage	10 V _{pp} (set at the 50Ω impedance)
Modulation bandwidth	$B_{\text{mod}} = 10 \text{ MHz}$
MultiCAP carrier number	$N = 10$
Carrier frequencies	0.5 to 9.5 MHz with a step size of 1 MHz
SRRC roll-off factor	$\beta = 0.15$
SRRC filter length	20 symbols
Baseband symbol rate	$R_s = 1/T_s = 869.57 \text{ kBaud}$
Bit-loading pattern	$\{k_n, n = 1, \dots, N\} = \{4 \ 5 \ 5 \ 5 \ 5 \ 5 \ 4 \ 4 \ 4\}$
Aggregate data rate	$R_b = \sum_{n=1}^N R_s k_n = 40 \text{ Mb/s}$
Distance	Up to 2 m

3. Challenges and Results

3.1. Flicker Issue and the DSP-based Solution

Flicker is a common problem in LED lighting, which is mainly caused by the low-frequency (ranging from 3 Hz to ~1 kHz) ripple of the current generated by the power driver in most cases [42]. Unlike the precise voltage sources used in our measurements, the commercial LED driver converts AC mains to a “noisy” DC current to drive the LED panel. For instance, the full-wave bridge rectifier or power factor correction (PFC) circuitry, which are two typical circuits widely adopted in commercial LED drivers, will generate ripples at twice the AC line frequency [42]. If not suppressed properly, the ripples can lead to severe flicker problems that cascade to data perturbations. Unfortunately, although the driving current from the commercial LED driver has been filtered to prevent the ripples from introducing noticeable flicker, the residual ripple amplitude is still quite high from the communication point of view. There are two major disadvantages: (i) the reduced modulation depth for VLC signals - since the VLC signal is superimposed onto the bias current, the headroom left for VLC signals is reduced if the bias current has a high ripple amplitude; (ii) the low-frequency flicker can interfere with the signal falling in the frequency range. The following two solutions help to combat the flicker issue:

1. A high-pass filter circuit can be inserted to filter out the low-frequency flicker if it is possible to modify the analogue frontend of the optical receiver.
2. If it is not feasible to change the hardware, DSP techniques can be used to remove the flicker by subtracting the low-frequency “envelope” from the received signal.

The first approach requires a hardware modification according to the specification of flicker and is not always feasible, while the second DSP approach is more flexible and can be applied universally. The detailed block diagram of the DSP solution is illustrated in Figure 8. The fundamental idea is to subtract the estimated flicker signal from the received signal $r(t)$. To recover the flicker signal, a low-pass finite impulse response (FIR) filter is used to filter out the low-frequency components. Before feeding $r(t)$ through the FIR filter, a decimation operation, or downsampling, is applied to decrease the sampling rate to reduce the implementation complexity of the succeeded FIR filter. After the FIR filter, an interpolation operation is paired to increase the sampling rate back to the original sampling rate.

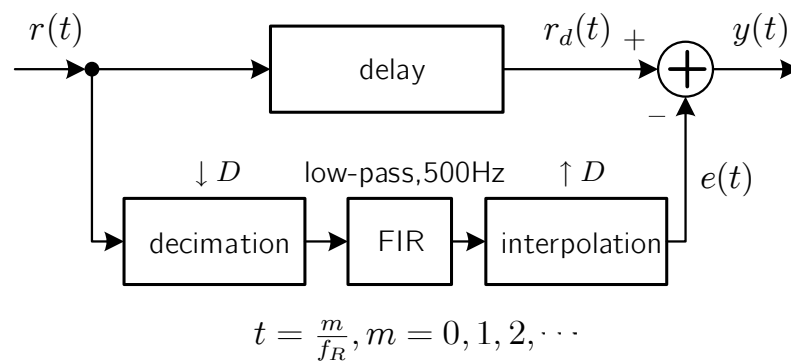


Figure 8. DSP-based solution to remove the flicker in the received signal. $r(t)$ is the signal captured directly by the OSC at a sample rate of f_R and $e(t)$ is the estimated low-frequency “envelope” signal for the flicker. $y(t)$ is flicker-free after the removal of $e(t)$ from $r(t)$.

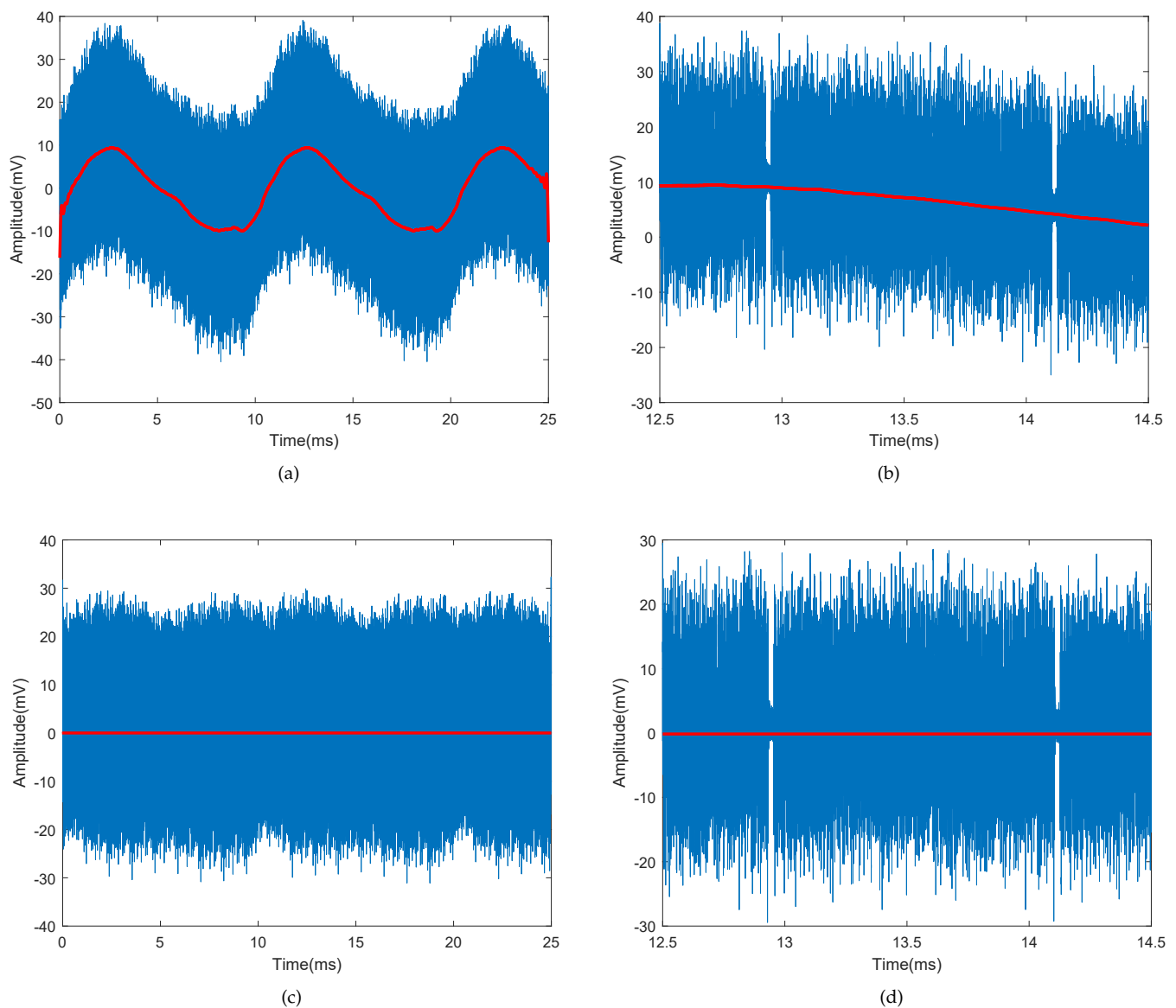


Figure 9. (a) Received signal $r(t)$ (blue) and the corresponding estimated flicker signal $e(t)$ (red); (b) a zoom-in view of a segment of $r(t)$ and $e(t)$; (c) filtered signal $y(t)$; (d) a zoom-in view of a segment of $y(t)$.

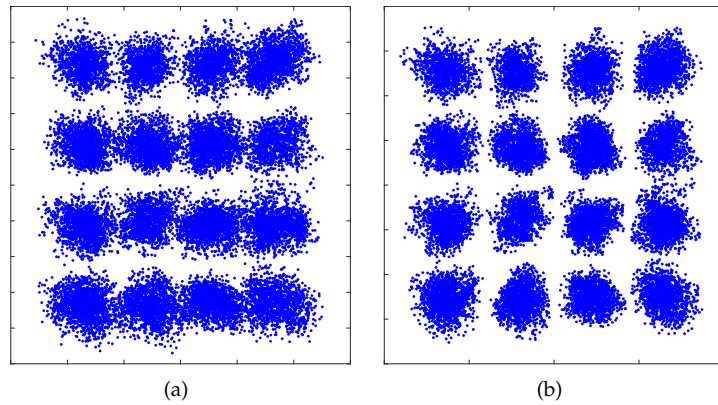


Figure 10. (a) Decoded constellation diagram at the 1st carrier before flicker removal; (b) Decoded constellation diagram at the 1st carrier after flicker removal;

Figure 9(a) shows the signal $r(t)$ in blue, which is captured by the OSC and exhibits a slowly changing envelope caused by the flicker. From the waveform, the period of the flicker can be roughly estimated to be around 10 ms, indicating a fundamental frequency of 100 Hz (twice the UK mains frequency). Since the flicker is not a perfect single-tone sine wave, a low-pass FIR filter with a cut-off frequency of 500 Hz is used to let a frequency up to the 5th harmonic pass through to recovery a close replica of the flicker. The filtered signal $e(t)$ is shown in red in Figure 9(a). A zoom-in view of $r(t)$ and $e(t)$ is also provided in Figure 9(b). It can be observed that the flicker $e(t)$ has been successfully extracted from $r(t)$ and corresponds to the fluctuating DC level. Once subtracted from $r(t)$, the flicker can be removed, and a stable DC level at around zero is achieved, as shown in Figure 9(c) and Figure 9(d). The improvement in BER performance can be clearly observed from the decoded constellation diagrams at the 1st carrier before and after flicker removal as shown in Figure 10. We also find that only the 1st carrier was affected, which confirms with our analysis that the flicker interferes with the sub-band using the same spectrum for data transmission.

3.2. Results and Discussion

The BER was measured at varying distances from 1 to 2 m, see Figure 11. For reference purposes, a light level (in lux) curve is also provided. Experimental results show that, with the proposed flicker removal DSP solution, a 40 Mb/s link can be supported up to 2 m with an illuminance level of ~300 lux (minimum illuminance for indoor workplaces in accordance with EN 12464-1 [43]), maintaining a BER below the 7% FEC limit. When the flicker removal algorithm was not applied, the system performance was mainly limited by the BER performance of the 1st sub-band and the overall BER level was close to the FEC limit with a narrow margin. The effectiveness of the flicker mitigation was validated by the improvement in the system performance and robustness.

To better demonstrate the system performance, the measured spectra of the received signal and background noise at a distance of 1.4 m (with a light level of 600 lux measured) are shown in Figure 12. The ten carriers can be clearly observed, with every recovered constellation diagram from each carrier included in Figure 13. The corresponding SNR curve is given in Figure 14 with the bit-loading pattern plotted. As mentioned earlier, the bit-loading pattern is determined at the longest distance and therefore the SNR profile at the distance of 1.4 m can support quite clear constellation diagrams as shown in Figure 13..

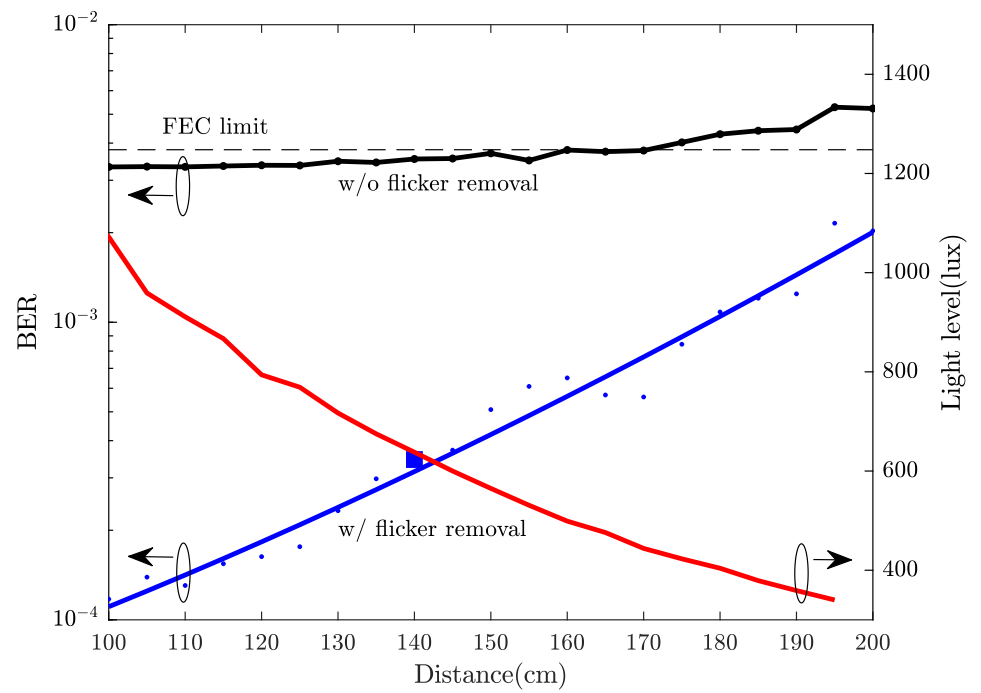


Figure 11. BER performance and light level vs distance.

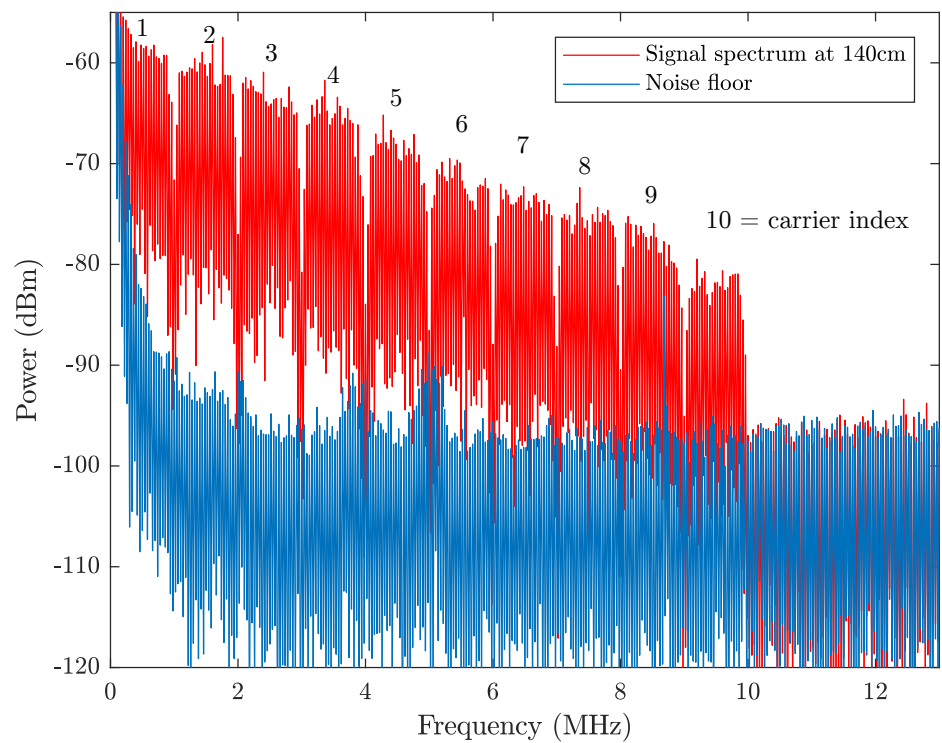


Figure 12. Measured signal spectrum and background noise spectrum at the distance of 1.4 metres.

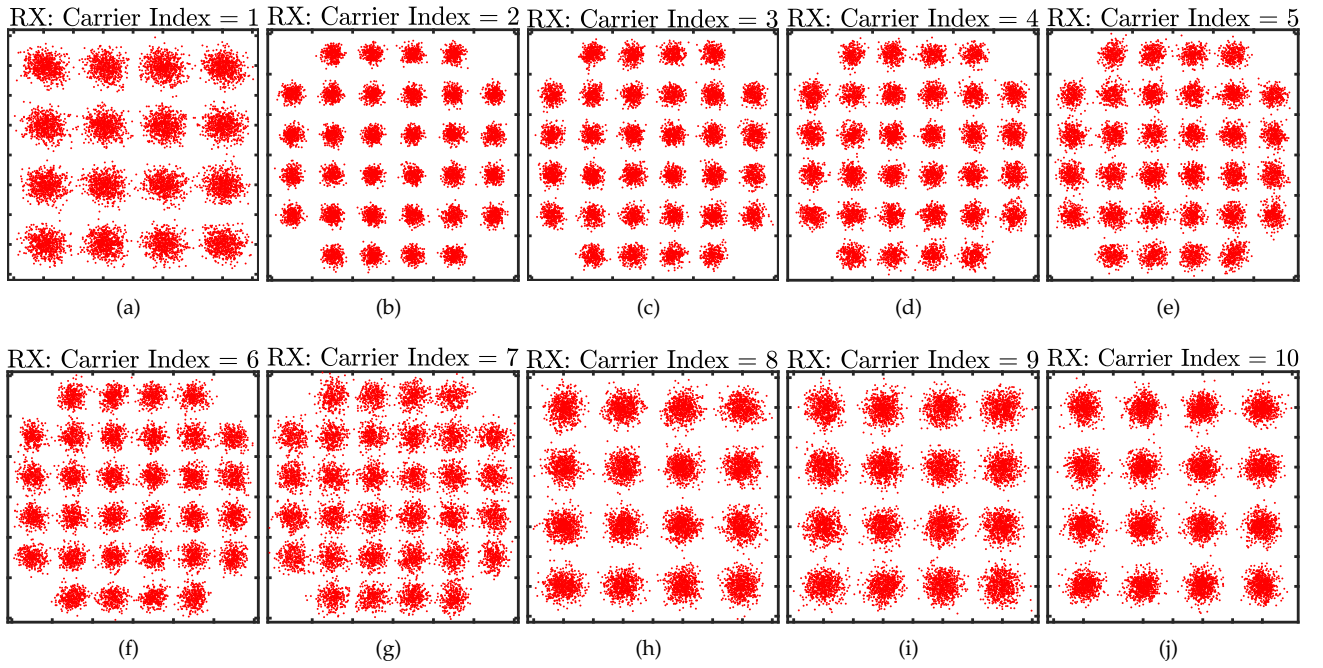


Figure 13. Demodulated constellation diagrams for each carrier at the distance of 1.4 metres.

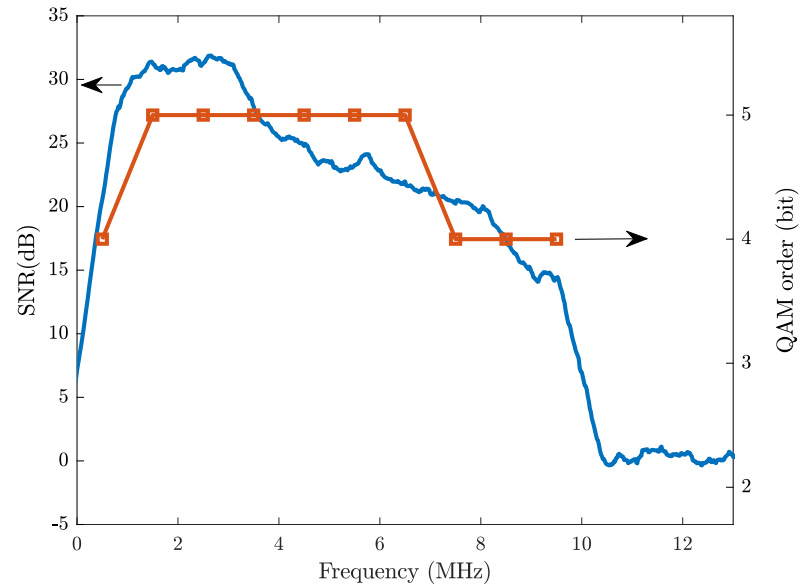


Figure 14. Measured SNR profile and the bit-loading pattern at the distance of 1.4 metres.

Two major limiting factors for achieving higher R_b using the off-the-shelf LED panel are observed. Firstly, the modulation bandwidth is limited to 10 MHz because severe distortion, which might be contributed by the LED's nonlinearity and the parasitic in the electronics, is incurred beyond 10 MHz. It could be a big issue when trying to reuse the existing lighting sources in the applications of high-speed VLC standards like G.9991 [18] requiring a minimum bandwidth of 50 MHz. Secondly, the flicker caused by the LED driver inevitably reduces the modulation depth or the transmitted optical power for VLC signals, imposing a limit on the SNR and the achievable R_b . Improvement in data rates is expected if the LED driver is optimised for VLC.

4. Conclusions

The feasibility of upgrading the existing indoor LED-based lighting infrastructure with add-on VLC functionality was validated by our demonstration system. With a bias-tee, a minimum modification was applied to the large LED panel installed in the ceiling to enable intensity modulation for simultaneous communication and illumination. A transmission rate of 40 Mb/s was supported up to 2 m with a measured illuminance level of ~300 lux. The key factors preventing our system from achieving higher data rates are the limited bandwidth of the LED panel and the flicker caused by the low-cost LED driver. To combat those issues, we utilised the low-complexity MultiCAP modulation to exploit the spectrum out of the 3-dB bandwidth and proposed a DSP-based solution to remove the baseline wander effect caused by the flicker.

Author Contributions: Conceptualisation, X.L. and Z.G.; methodology, X.L.; software, X.L. and P.A.H.; validation, X.L.; writing—original draft preparation, X.L.; writing—review and editing, Z.G., S.Z. and P.A.H. All authors have read and agreed to the published version of the manuscript.

Funding: This work was supported by the European Union’s Horizon 2020 Research and Innovation Programme, under the Marie Skłodowska-Curie grant agreement no 764461 (VisIoN).

Institutional Review Board Statement: Not applicable.

Informed Consent Statement: Not applicable.

Conflicts of Interest: The authors declare no conflicts of interest. The funders had no role in the design of the study; in the collection, analyses, or interpretation of data; in the writing of the manuscript; or in the decision to publish the results.

References

1. Ghassemlooy, Z.; Alves, L.N.; Zvanovec, S.; Khalighi, M.A. *Visible Light Communications: Theory and Applications*; CRC Press, 2017.
2. Uysal, M.; Capsoni, C.; Ghassemlooy, Z.; Boucouvalas, A.; Udvary, E. *Optical Wireless Communications: An Emerging Technology*; Springer, 2016.
3. Rehman, S.U.; Ullah, S.; Chong, P.H.J.; Yongchareon, S.; Komosny, D. Visible Light Communication: A System Perspective—Overview and Challenges. *Sensors* **2019**, *19*. doi:10.3390/s19051153.
4. Steigerwald, D.A.; Bhat, J.C.; Collins, D.; Fletcher, R.M.; Holcomb, M.O.; Ludowise, M.J.; Martin, P.S.; Rudaz, S.L. Illumination with solid state lighting technology. *IEEE Journal of Selected Topics in Quantum Electronics* **2002**, *8*, 310–320.
5. Haigh, P.A.; Ghassemlooy, Z.; Le Minh, H.; Rajbhandari, S.; Arca, F.; Tedde, S.F.; Hayden, O.; Papakonstantinou, I. Exploiting Equalization Techniques for Improving Data Rates in Organic Optoelectronic Devices for Visible Light Communications. *Journal of Lightwave Technology* **2012**, *30*, 3081–3088.
6. Haigh, P.A.; Ghassemlooy, Z.; Rajbhandari, S.; Papakonstantinou, I. Visible light communications using organic light emitting diodes. *IEEE Communications Magazine* **2013**, *51*, 148–154. doi:10.1109/MCOM.2013.6576353.
7. Nazari Chaleshtori, Z.; Ghassemlooy, Z.; Eldeeb, H.B.; Uysal, M.; Zvanovec, S. Utilization of an OLED-Based VLC System in Office, Corridor, and Semi-Open Corridor Environments. *Sensors* **2020**, *20*.
8. Chi, Y.C.; Hsieh, D.H.; Lin, C.Y.; Chen, H.Y.; Huang, C.Y.; He, J.H.; Ooi, B.; DenBaars, S.P.; Nakamura, S.; Kuo, H.C.; Lin, G.R. Phosphorous Diffuser Diverged Blue Laser Diode for Indoor Lighting and Communication. *Scientific Reports* **2015**, *5*, 18690. doi:10.1038/srep18690.
9. Zafar, F.; Bakaul, M.; Parthiban, R. Laser-Diode-Based Visible Light Communication: Toward Gigabit Class Communication. *IEEE Communications Magazine* **2017**, *55*, 144–151.
10. Liu, C.B.; Sadeghi, B.; Knightly, E.W. Enabling vehicular visible light communication (V2LC) networks. Proceedings of the Eighth ACM international workshop on Vehicular inter-networking, 2011, pp. 41–50.
11. Marabissi, D.; Mucchi, L.; Caputo, S.; Nizzi, F.; Pecorella, T.; Fantacci, R.; Nawaz, T.; Seminara, M.; Catani, J. Experimental Measurements of a Joint 5G-VLC Communication for Future Vehicular Networks. *Journal of Sensor and Actuator Networks* **2020**, *9*. doi:10.3390/jsan9030032.
12. Caputo, S.; Mucchi, L.; Cataliotti, F.; Seminara, M.; Nawaz, T.; Catani, J. Measurement-based VLC channel characterization for I2V communications in a real urban scenario. *Vehicular Communications* **2020**, p. 100305. doi:https://doi.org/10.1016/j.vehcom.2020.100305.
13. Nawaz, T.; Seminara, M.; Caputo, S.; Mucchi, L.; Catani, J. Low-Latency VLC System with Fresnel Receiver for I2V ITS Applications. *Journal of Sensor and Actuator Networks* **2020**, *9*. doi:10.3390/jsan9030035.
14. Khan, L.U. Visible light communication: Applications, architecture, standardization and research challenges. *Digital Communications and Networks* **2017**, *3*, 78–88.

15. Jungnickel, V.; Hinrichs, M.; Bober, K.L.; Kottke, C.; Corici, A.A.; Emmelmann, M.; Rufo, J.; Bök, P.; Behnke, D.; Riege, M.; Wu, X.; Singh, R.; Brien, D.C.O.; Collins, S.; Faulkner, F.; Vazquez, M.M.; Bech, M.C.; Geilhardt, F.; Braun, R.; Deng, X.; Tangdionga, E.; Koonen, A.M.J. Enhance Lighting for the Internet of Things. Global LIFI Congress (GLC), 2019, pp. 1–6.
16. Béchadargue, B.; Azoulay, B. An Industrial View on LiFi Challenges and Future. 12th International Symposium on Communication Systems, Networks and Digital Signal Processing (CSNDSP), 2020, pp. 1–6.
17. Haas, H.; Yin, L.; Wang, Y.; Chen, C. What is LiFi? *Journal of Lightwave Technology* **2016**, *34*, 1533–1544.
18. ITU-T. G.9991 : High-speed indoor visible light communication transceiver – System architecture, physical layer and data link layer specification **2019**.
19. Oksman, V.; Galli, S. G.hn: The new ITU-T home networking standard. *IEEE Communications Magazine* **2009**, *47*, 138–145.
20. ITU-T. G.9961 : Unified high-speed wireline-based home networking transceivers - Data link layer specification **2018**.
21. Sturniolo, A.; Cossu, G.; Messa, A.; Ciaramella, E. Ethernet over commercial lighting by a Visible Light Communication. 2018 Global LIFI Congress (GLC), 2018, pp. 1–4.
22. Chvojka, P.; Burton, A.; Pesek, P.; Li, X.; Ghassemlooy, Z.; Zvanovec, S.; Anthony Haigh, P. Visible light communications: increasing data rates with polarization division multiplexing. *Optics Letters* **2020**, *45*, 2977–2980. doi:10.1364/OL.392167.
23. Hu, F.; Li, G.; Zou, P.; Hu, J.; Chen, S.; Liu, Q.; Zhang, J.; Jiang, F.; Wang, S.; Chi, N. 20.09-Gbit/s Underwater WDM-VLC Transmission based on a Single Si/GaAs-Substrate Multichromatic LED Array Chip. Optical Fiber Communications Conference and Exhibition (OFC), 2020, pp. 1–3.
24. Bian, R.; Tavakkolnia, I.; Haas, H. 15.73 Gb/s Visible Light Communication With Off-the-Shelf LEDs. *Journal of Lightwave Technology* **2019**, *37*, 2418–2424. doi:10.1109/JLT.2019.2906464.
25. Burton, A.; Bentley, E.; Minh, H.L.; Ghassemlooy, Z.; Aslam, N.; Liaw, S.K. Experimental demonstration of a 10BASE-T Ethernet visible light communications system using white phosphor light-emitting diodes. *IET Circuits, Devices & Systems* **2014**, *8*, 322–330. doi:10.1049/iet-cds.2013.0359.
26. Sung, J.Y.; Chow, C.W.; Yeh, C.H. Is blue optical filter necessary in high speed phosphor-based white light LED visible light communications? *Optics Express* **2014**, *22*, 20646–20651. doi:10.1364/OE.22.020646.
27. Li, H.; Chen, X.; Guo, J.; Chen, H. A 550 Mbit/s real-time visible light communication system based on phosphorescent white light LED for practical high-speed low-complexity application. *Optics Express* **2014**, *22*, 27203–27213. doi:10.1364/OE.22.027203.
28. Huang, X.; Wang, Z.; Shi, J.; Wang, Y.; Chi, N. 1.6 Gbit/s phosphorescent white LED based VLC transmission using a cascaded pre-equalization circuit and a differential outputs PIN receiver. *Optics Express* **2015**, *23*, 22034–22042. doi:10.1364/OE.23.022034.
29. Li, X.; Ghassemlooy, Z.; Zvanovec, S.; Jimenez, R.P.; Haigh, P. Should Analogue Pre-equalisers be Avoided in VLC Systems? *IEEE Photonics Journal* **2020**, pp. 1–1. doi:10.1109/JPHOT.2020.2966875.
30. Haigh, P.A.; Darwazeh, I. Real-Time Experimental Demonstration of Multi-band CAP Modulation in a VLC System with Off-the-Shelf LEDs. IEEE INFOCOM 2019 - IEEE Conference on Computer Communications Workshops (INFOCOM WKSHPS), 2019, pp. 1001–1002. doi:10.1109/INFOCOMW.2019.8845128.
31. Haigh, P.A.; Burton, A.; Werfli, K.; Minh, H.L.; Bentley, E.; Chvojka, P.; Popoola, W.O.; Papakonstantinou, I.; Zvanovec, S. A Multi-CAP Visible-Light Communications System With 4.85-b/s/Hz Spectral Efficiency. *IEEE Journal on Selected Areas in Communications* **2015**, *33*, 1771–1779. doi:10.1109/JSAC.2015.2433053.
32. Haigh, P.A.; Le, S.T.; Zvanovec, S.; Ghassemlooy, Z.; Luo, P.; Xu, T.; Chvojka, P.; Kanesan, T.; Giacomidis, E.; Canyelles-Pericas, P.; Minh, H.L.; Popoola, W.; Rajbhandari, S.; Papakonstantinou, I.; Darwazeh, I. Multi-band carrier-less amplitude and phase modulation for bandwidth limited visible light communications systems. *IEEE Wireless Communications* **2015**, *22*, 46–53. doi:10.1109/MWC.2015.7096284.
33. Wu, F.M.; Lin, C.T.; Wei, C.C.; Chen, C.W.; Chen, Z.Y.; Huang, H.T.; Chi, S. Performance Comparison of OFDM Signal and CAP Signal Over High Capacity RGB-LED-Based WDM Visible Light Communication. *IEEE Photonics Journal* **2013**, *5*, 7901507–7901507. doi:10.1109/JPHOT.2013.2271637.
34. Deng, X.; Arulandu, K.; Wu, Y.; Zhou, G.; Linnartz, J.M.G. Performance Analysis for Joint Illumination and Visible Light Communication Using Buck Driver. *IEEE Transactions on Communications* **2018**, *66*, 2065–2078.
35. Gao, Y.; Li, L.; Mok, P.K.T. An AC Input Inductor-Less LED Driver for Efficient Lighting and Visible Light Communication. *IEEE Journal of Solid-State Circuits* **2018**, pp. 1–13.
36. Deng, X.; Arulandu, K.; Wu, Y.; Mardanikorian, S.; Zhou, G.; Linnartz, J.M.G. Modeling and Analysis of Transmitter Performance in Visible Light Communications. *IEEE Transactions on Vehicular Technology* **2019**, *68*, 2316–2331.
37. Li, X.; Ghassemlooy, Z.; Zvanovec, S.; Haigh, P.A. Experimental Demonstration of a 40 Mb/s VLC System Using a Large Off-the-Shelf LED Panel. 2020 12th International Symposium on Communication Systems, Networks and Digital Signal Processing (CSNDSP), 2020, pp. 1–5. doi:10.1109/CSNDSP49049.2020.9249608.
38. Li, X.; Ghassemlooy, Z.; Zvanovec, S.; Zhang, M.; Burton, A. Equivalent Circuit Model of High Power LEDs for VLC Systems. 2nd West Asian Colloquium on Optical Wireless Communications (WACOWC), 2019, pp. 90–95.
39. Mana, S.M.; Hellwig, P.; Hilt, J.; Berenguer, P.W.; Jungnickel, V. Experiments in Non-Line-of-Sight Li-Fi Channels. Global LIFI Congress (GLC), 2019, pp. 1–6.
40. Eldeeb, H.B.; Uysal, M.; Mana, S.M.; Hellwig, P.; Hilt, J.; Jungnickel, V. Channel Modelling for Light Communications: Validation of Ray Tracing by Measurements. 2020 12th International Symposium on Communication Systems, Networks and Digital Signal Processing (CSNDSP), 2020, pp. 1–6. doi:10.1109/CSNDSP49049.2020.9249565.

-
41. Olmedo, M.I.; Zuo, T.; Jensen, J.B.; Zhong, Q.; Xu, X.; Popov, S.; Monroy, I.T. Multiband Carrierless Amplitude Phase Modulation for High Capacity Optical Data Links. *Journal of Lightwave Technology* **2014**, *32*, 798–804.
 42. Society, I.P.E. IEEE Recommended Practices for Modulating Current in High-Brightness LEDs for Mitigating Health Risks to Viewers **2015**.
 43. for Standardization, E.C. Light and lighting—lighting of work places—Part 1: indoor work places. *BSI Standard Publication, page 10. EN* **2011**, 12464.